# Molecular basis of hydroperoxide specificity in peroxiredoxins: the case of AhpE from Mycobacterium tuberculosis



| | |
|---|---|
| Journal: | *Biochemistry* |
| Manuscript ID | bi-2015-00758f.R2 |
| Manuscript Type: | Article |
| Date Submitted by the Author: | 11-Nov-2015 |





| | |
|---|---|
| Complete List of Authors: | Zeida, Ari; Facultad de Ciencias Exactas y Naturales, University of Buenos Aires, INQUIMAE-Dpto. Quimica Inorganica, Analitica y Quimica Fisica<br>Reyes, Anibal; Facultad de Medicina, UdelaR, Bioquímica<br>Lichtig, Pablo; Facultad de Ciencias Exactas y Naturales, University of Buenos Aires, INQUIMAE-Dpto. Quimica Inorganica, Analitica y Quimica Fisica<br>Hugo, Martín; Facultad de Medicina, UdelaR, Bioquímica<br>Vazquez, Diego; University Of Buenos Aires, Department of Biological Chemistry and Institute of Biochemistry and Biophysics (IQUIFIB), School of Pharmacy and Biochemisrty<br>Santos, Javier; University of Buenos Aires, Department of Biological Chemistry and Institute of Biochemistry and Biophysics (IQUIFIB), School of Pharmacy and Biochemistry<br>Gonzalez Flecha, F Luis; Universidad de Buenos Aires, Department of Biological Chemistry<br>Radi, Rafael; Facultad de Medicina, Bioquímica<br>Estrin, Dario; University of Buenos Aires, Facultad de Ciencias Exactas y Naturales, Quimica Inorganica, Analitica y Quimica Fisica<br>Trujillo, Madia; Facultad de Medicina, Bioquímica |
| | |

# Molecular basis of hydroperoxide specificity in peroxiredoxins: the case of AhpE from *Mycobacterium tuberculosis*

*Ari Zeida,[a‡] Aníbal M. Reyes,[b‡] Pablo Lichtig,[a] Martín Hugo,[b†] Diego S. Vazquez,[c] Javier Santos,[c] F. Luis González Flecha,[c] Rafael Radi,[b] Dario A. Estrin,[a*] Madia Trujillo[b*]*

[a] Departamento de Química Inorgánica, Analítica y Química-Física and INQUIMAE-CONICET, Facultad de Ciencias Exactas y Naturales, Universidad de Buenos Aires, Buenos Aires, Argentina.

[b] Departamento de Bioquímica and Center for Free Radical and Biomedical Research, Facultad de Medicina, Universidad de la República, Montevideo, Uruguay.

[c] IQUIFIB (UBA-CONICET) and Departamento de Química Biológica, Facultad de Farmacia y Bioquímica, Universidad de Buenos Aires, Argentina.

KEYWORDS

peroxiredoxins, peroxides, substrate specificity, activation parameters, transition state

ABSTRACT

Peroxiredoxins (Prxs) constitute a ubiquitous family of Cys-dependent peroxidases that play essential roles in reducing hydrogen peroxide, peroxynitrite and organic hydroperoxides in almost all organisms. Members of the Prx subfamilies show differential oxidizing substrate specificities that await explanations at a molecular level. Among them, alkyl hydroperoxide reductases E (AhpE) is a novel subfamily comprising *Mycobacterium tuberculosis* AhpE and AhpE-like proteins expressed in some bacteria and archaea. We previously reported that *Mt*AhpE reacts ~$10^4$ times faster with an arachidonic acid-derived hydroperoxide than with hydrogen peroxide, and suggested that this surprisingly high reactivity was related to the presence of a hydrophobic groove at the dimer interface evidenced in the crystallography structure of the enzyme. In this contribution we experimentally confirmed the existence of an exposed hydrophobic patch in *Mt*AhpE. We found that fatty acid hydroperoxide reduction by the enzyme showed positive activation entropy that importantly contributed to catalysis. Computational dynamics indicated that interactions of fatty acid-derived hydroperoxides with the enzyme properly accommodated them inside the active site and modifies enzyme´s dynamics. The computed reaction free energy profile obtained via QM/MM simulations is consistent with a greater reactivity in comparison with hydrogen peroxide. This study represents new insights on the understanding of the molecular basis that determines oxidizing substrate selectivity in the peroxiredoxin family, which has not been investigated at an atomic level so far.

## INTRODUCTION

Peroxiredoxins (Prxs) are ubiquitous and usually highly abundant thiol-dependent peroxidases that play key roles in cellular antioxidant defenses as well as in redox signaling processes including those involved in cell proliferation, senescence and apoptosis.[1-6] As a consequence, Prxs constitute potential drug targets for the treatment of diseases such as infections and cancer, where the peroxide detoxification and/or signaling actions of Prxs are involved.[7-11] Molecular-targeted drug design requires a precise knowledge of the mechanisms of catalysis, which at present have only started to be unraveled.

Prxs catalyze the reduction of different peroxides such as hydrogen peroxide ($H_2O_2$), organic hydroperoxides and peroxynitrite.[12, 13] In most cases, the reducing substrate is thioredoxin or a thioredoxin-related protein. The enzymes follow a bi-substrate double displacement (or ping-pong) mechanism, involving at least one critical cysteine residue, the peroxidatic cysteine, which has a low thiol $pK_a$ value, typically $\leq 6.3$.[14] During the catalytic cycle the thiolate at the reduced peroxidatic cysteine residue ($Cys_{P\text{-}S^-}$) is firstly oxidized to sulfenate ($Cys_{P\text{-}SO^-}$) by the peroxide substrate (ROOH) releasing the corresponding alcohol (ROH). Sulfenate reduction then occurs by different routes, depending on whether a second, resolving cysteine residue is required (2-Cys Prxs) or not (1-Cys Prxs) for enzymatic activity.[15] Briefly, in 2-Cys Prxs the resolving Cys reacts with the sulfenate at $Cys_P$ to form a disulfide bond, which is latter reduced by thioredoxin. On the contrary, sulfenate in oxidized 1-Cys Prxs interacts directly with the reducing substrate(s).[12] More recently, it has been demonstrated that oxidized forms of particular Prxs promote specific signaling protein oxidations, allowing them to respond indirectly to increased hydroperoxide concentrations.[16]

We are particularly interested in the oxidizing part of the catalytic cycle, trying to contribute to the understanding of a) the protein factors that make thiolates in $Cys_P$ of Prxs to react $10^3$ -$10^7$ faster with hydroperoxides than the thiolate in free cysteine (which represents the uncatalyzed reaction); b) the variable oxidizing substrate specificities displayed by the different Prx subfamilies. In general, peroxide-mediated thiolate oxidations occur through a nucleophilic sustitution $S_N2$ mechanism.[17] In the case of $H_2O_2$ reduction by a model thiolate as well as by the thiolate in $Cys_P$ of Prxs, the reaction occurs through a $S_N2$ mechanism accompanied by a proton transfer from the proximal hydroperoxide oxygen atom ($O_A$) to the distal oxygen ($O_B$), yielding water and sulfenate as products (Scheme 1).[18, 19]

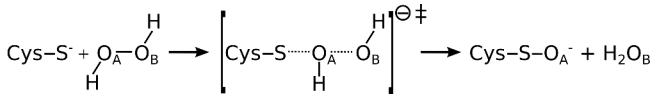


**Scheme 1.** Reduction of $H_2O_2$ by thiols.

The analysis of the crystallography structure of Prxs from different subfamilies co-crystallized with $H_2O_2$, water or peroxide-mimicking compounds bound to the active site indicated that transition state stabilization through a complex network of hydrogen bonds was the responsible for the enhanced $Cys_P$ reactivity in Prxs.[20] This was consistent with an important contribution of decreased activation enthalpy to the enhanced rate of $H_2O_2$ reduction by a model of Prx 2 and 3 active sites,[21] as well as by the 1-Cys Prx alkyl hydroperoxide reductase E from *Mycobacterium tuberculosis* (*Mt*AhpE), compared to the uncatalyzed reaction.[18, 19] The free energy profile of the latter reaction obtained by QM/MM calculations allowed a description of the electrostatic interactions and hydrogen bonds responsible for transition state stabilization at the atomic level.[19] Later on, QM/MM analysis indicated that in *Hs*PrxV, enhancement of specific nucleophilicity of the $Cys_P$ thiolate upon peroxide binding participate in catalysis of $H_2O_2$

reduction.[22] It is worth to note that, in spite of active site conservation, the rate constants of $H_2O_2$ reduction among Prx subfamilies (http://csb.wfu.edu/prex/)[23, 24] differ in several orders of magnitude. Differences in reactivity could arise either from subtle differences in the catalytic mechanisms (still to be identified) and/or from the existence of reactive or unreactive conformers in rapid equilibrium in different proportions among the Prx subfamilies. Indeed, NMR indicated that reduced PrxQ from *Arabidopsis thaliana* experienced rapid conformational changes that could influence its activity.[25]

Low molecular weight thiolates as well as non-peroxidatic protein thiolates are more reactive towards the peroxides with the lower leaving group p$K_a$, *i.e.* that of the ROH formed as product.[26] On the contrary, peroxide selectivity differs among Prx subfamilies. For example, reported rate constants for $H_2O_2$ and peroxynitrous acid reduction by thiolate in $Cys_P$ from the Prx1-AhpC subfamily (typical 2-Cys Prxs) are similar or even higher for $H_2O_2$, in spite of nitrite being a better leaving group than $OH^-$.[27-31] Moreover, *Hs*PrxV reduction of peroxynitrous acid is ~$10^3$ fold faster than $H_2O_2$ reduction, in agreement with the above mentioned expected tendency; however, reduction of artificial organic hydroperoxides *tert*-butyl hydroperoxide (*t*-BuOOH) and cumene hydroperoxide (CumeneOOH) were much faster than expected according to the corresponding alcohol p$K_a$s.[32, 33] These organic hydroperoxides were also ~100 fold more reactive than $H_2O_2$ with members of the thiol peroxidase (Tpx) subfamily.[34] In both *Hs*PrxV and Tpx subfamilies, increased reactivities towards organic hydroperoxides have been related to the presence of a hydrofobic collar of apolar side chains around their active site that could better interact with these substrates,[35] as initially suggested from the crystallography structure of *Hs*PrxV that co-crystalized with benzoate in close proximity to the active site

pocket.[36] However, the molecular basis of the oxidizing substrate specificities in Prxs, as well as in other thiol-dependent peroxidases,[37] are still unknown.

In the case of *Mt*AhpE, that belongs to the AhpE Prx subfamily expressed in some bacteria, reactivities with fatty acid hydroperoxides are extremely fast, with rate constants in the $10^8$ $M^{-1}s^{-1}$ range, being $10^3$-$10^4$ fold higher than with $H_2O_2$.[38, 39] Based on the reported structure of the enzyme,[40] we have previously suggested that a superficial hydrophobic groove present in the intersubunit interface of the dimeric enzyme could facilitate the interaction of *Mt*AhpE with fatty acid hydroperoxides.[39]

Herein, we present a combination of kinetics and equilibrium experiments combined with classical and hybrid QM/MM computer simulations, in order to understand the hydroperoxide selectivity of *Mt*AhpE at the molecular level. Results confirmed the existence of a surface exposed hydrophobic patch that could assist in properly locate fatty acid-derived hydroperoxides. Moreover, we found that protein-substrate interaction significantly modifies protein dynamics, probably favoring the anchorage of the enzyme in a reactive conformation. Although we observed the same overall reaction mechanism for *Mt*AhpE-dependent reduction of fatty acid hydroperoxides as we previously reported for $H_2O_2$,[19] thermodynamic activation parameters of the reaction strongly differ between both oxidizing substrates and are consistent with an important contribution of activation entropy to catalysis of fatty acid hydroperoxide oxidation.

## EXPERIMENTAL and COMPUTATIONAL PROCEDURES

### *Chemicals*

1-anilino-8-naphthalene sulfonate (ANS) was from Molecular Probes. 1,4-dithiothreitol (DTT), and diethylenetriaminepentaacetic acid (dtpa) were purchased from Sigma-Aldrich. 12S-hydroperoxy-5Z,8Z,10E,14Z-eicosatetraenoic-5,6,8,9,11,12,14,15-d8 acid (12-HpETE), 4-hydroxy-2E-nonenal (4-HNE), and 4-hydroperoxy-2E-nonenal (4-HpNE) were obtained from Cayman Chemicals.

### *Protein expression and purification*

*Mt*AhpE (TB Data-base gene name Rv2238c) was expressed in *Escherichia coli* BL21(DE3) (expression vector pDEST17) as a recombinant His-tagged protein and purified as previously described.[40] The concentration of the protein was determined spectrophotometrically at 280 nm, using a molar absorption coefficient of 23,950 $M^{-1}cm^{-1}$, calculated according to protein sequence using the ProtParam tool in ExPASy,http://web.expasy.org/protparam/.[41] All experiments were performed in 100 mM sodium phosphate buffer plus 0.1 mM dtpa pH 7.4 and 25ºC, unless otherwise indicated.

### *Kinetic measurements of MtAhpE oxidation*

The rate constants of *Mt*AhpE oxidation by 4-HpNE and 12-HpETE were determined by following the decrease in protein intrinsic fluorescence intensity ($\lambda_{exc}$ = 295 nm) that occurred upon protein oxidation. Typically reduced *Mt*AhpE (0.1 μM) was rapidly mixed with the hydroperoxide in excess using a stopped-flow equipment (Applied Photophysics SX20) as previously described.[38] Observed rate constants of fluorescence decrease ($k_{obs}$) were determined

by fitting a single exponential function to the experimental data, and second-order rate constants for the reactions were obtained from the slope of the plot of $k_{obs}$ *versus* peroxide concentration. Alternatively, second-order oxidation rate constants were determined by fitting the *pseudo*-first order integrated rate equation to the whole data set. As 4-HpNE is an aldehyde which could react as an electrophile with cysteine or other nucleophilic residues in proteins,[42] we performed control experiments mixing *Mt*AhpE with 4-HNE. In order to obtain the thermodynamic activation parameters of *Mt*AhpE oxidation by 12-HpETE, the experiment was performed at four different temperatures (ranging from 8°C to 25°C). Temperature range was limited to ≤25ºC due to the fact that reaction rates were too fast to be followed in our stopped-flow equipment (mixing time < 1.1 ms) at higher temperatures, even using 0.1 μM enzyme and ≤ 2 μM 12-HpETE. Activation enthalpy ($\Delta H^{\ddagger}$) and entropy ($\Delta S^{\ddagger}$) were obtained from the slope and intercepts of the Eyring plot, respectively, using the Eyring equation.

*ANS fluorimetric assays*

Fluorescence measurements were performed using a Jasco FP-6500 spectrofluorometer in a 3 × 3 mm quartz cuvette. Both excitation and emission band-widths were set at 4 nm. Excitation was performed at 295 nm to excite protein tryptophan (Trp) residues and/or 380 nm to excite ANS. The Förster Resonance Energy Transfer (FRET) efficiency was determined by registering the total fluorescence intensity of the Trp residues of *Mt*AhpE (in the presence of 1 mM DTT) after adding increasing concentration of ANS. The experiment was repeated at three different concentrations of *Mt*AhpE (1.5 μM, 3 μM and 8 μM). Assuming identical and independent binding sites, the resulting relative decrease of total fluorescence can be described by:

$$1-\frac{F}{F_0}=\frac{-1-K_a[AhpE]_T x-nK_a[AhpE]_T-\sqrt{(1+K_a[AhpE]_T x+nK_a[AhpE]_T)^2-4nK_a^2[AhpE]_T^2 x}}{-2K_a[AhpE]_T} \quad \text{(equation 1)}$$

where $F$ is the total fluorescence, $F_0$ correspond to the fluorescence intensity of *Mt*AhpE in the absence of ANS, $K_a$ is the association constant, $n$ is the stoichiometric coefficient of ANS per *Mt*AhpE monomer and $x = \frac{[ANS]_T}{[AhpE]_T}$. This equation was initially fitted independently for each *Mt*AhpE concentration, and afterwards a global fit was performed (where equation 1 was fitted to the whole set of data).

*Docking and classical molecular dynamics*

The crystal structure of *Mt*AhpE dimer in the reduced state (PDBid: 1XXU)[40] was used as starting structure. $Cys_P$ (p$K_a$= 5.2)[38] was assumed to be in the reactive deprotonated form. The system was solvated using a default method, with a octahedral box of 12 Å in radius with TIP3P water molecules.[43] All used residue parameters correspond to the parm99 Amber force field,[44] except for the peroxides substrates, which were developed by a standard procedure: partial charges were computed using the restricted electrostatic potential (RESP) recipe and DFT electronic structure calculations with the PBE functional and *dzvp* basis set. Equilibrium distances and angles, as well as force constants, were computed using the same methods and basis set used for computed charges.

In order to obtain *Mt*AhpE:peroxide complex initial structures, we performed a biased docking experiment[45] for the 15-HpETE substrate using the information previously obtained for the interaction of $H_2O_2$ within the enzyme active-site.[19] Therefore, the position of the peroxide moiety was fixed, and the rest of the molecule was docked and standard annealing was then performed. Initial structures for *Mt*AhpE:*t*-BuOOH and *Mt*AhpE:4-HpNE complexes were then obtained from seemingly well docked structures of *Mt*AhpE:15-HpETE complex. All simulations were performed using periodic boundary conditions with a 10 Å cutoff and particle

mesh Ewald (PME) summation method for treating the electrostatic interactions. The hydrogen bond lengths were kept at their equilibrium distance by using the SHAKE algorithm, while temperature and pressure were kept constant with a Langevin thermostat and barostat, respectively, as implemented in the AMBER12 program.[44] In every case, the system was optimized in 1000 steps (10 with steep gradient and the rest with conjugate gradient). Then, it was slowly heated from 0 K to 300 K for 20 ps at constant pressure, with Berendsen thermostat, and pressure was equilibrated at 1 bar for 5 ps. After these two steps, a 10 ns MD long simulation at constant temperature (300 K) and constant volume was performed. Free molecular dynamics at the NPT ensemble were performed for each substrate (i.e. 15-HpETE, 4-HpNE, *t*-BuOOH and $H_2O_2$). Afterwards, two sets of 100 ns trajectories were performed in which a "wall-like" restraint was applied, biasing sulfur atom and peroxidatic oxygen atom distance to be less than 3.5 or 10 Å. Binding free energy calculations were performed at the MM/GBSA level,[46] selecting 200 structures with a distance between reactive atoms of less than or equal to 3.5 Å. The same set of structures was used to calculate the difference in solvent accessible surface area (SASA) upon binding of the substrates, defined as:

$$\Delta SASA = SASA_{MtAhpE:ROOH} - (SASA_{MtAhpE} + SASA_{ROOH}) \quad \text{(equation 2)}$$

*Hybrid QM/MM simulations*

QM/MM simulations were carried out using our own developed code[47, 48] with similar protocols and parameters as were used previously.[18, 19] This scheme was constructed by partitioning the system into QM and MM subsystems. The QM system consisted in the $H_3COOH$ moiety of 15-HpETE (two of the H atoms of the methyl group being the link atoms with the MM system) together with $Cys_{45}$ ($Cys_P$) and $Arg_{116}$ sidechains. We employed the scaled position link atom to

describe the QM/MM boundaries.[49] For the QM region, computations were performed at the generalized gradient approximation (GGA) level, using the PBE combination of exchange and correlation functionals, with a *dzvp* basis set for the expansion of the one-electron orbitals. The electronic density was also expanded in an auxiliary basis set and the coefficients for the fitting were computed by minimizing the error in the Coulomb repulsion energy.

To explore reaction's free energy and mechanism, we employed an umbrella sampling scheme, choosing as reaction coordinate the difference between the $O_A-O_B$ and the $S_P-O_A$ distances (see Supplementary Information Table S2), which was sampled from -1.7 to 1.2 Å, divided in 31 simulation windows, using harmonic potential constants of 200 kcal $mol^{-1}$ $Å^{-2}$. The selection of the QM region and the reaction coordinate, have been shown to provide a realistic representation of the reaction mechanism in previous works.[18, 19] Specifically, on the basis of structural and energetic considerations, we have shown that water molecules are not directly involved in the reaction. Initial configurations were generated from preliminary 2 ns classical equilibration runs in which the solute was treated classically as a rigid moiety, followed by a 2 ps QM/MM MD trajectory. For each window, QM/MM MD simulations were run for at least 10 ps. We employed the Verlet algorithm to integrate Newton's equations with a time step of 1 fs. During the simulations, the temperature was held constant at 300 K using the Langevin thermostat. The free energy profile was obtained using both simple reweighting and umbrella integration methods,[50] with almost identical results. Statistical errors on activation and reaction free energies were calculated as suggested by Kästner and coworkers.[51]

All dynamics visualizations and molecular drawings were performed with VMD 1.9.1.[52]

RESULTS and DISCUSSION

*Reduction of peroxides by MtAhpE*

In order to evaluate whether the reactivity of fatty-acid derived hydroperoxides is dependent on the length of the aliphatic tail, we determined the second order rate constant of the reduction of 4-HpNE by *Mt*AhpE as was previously done for a variety of substrates.[38, 39] No reaction was observed with 4-HNE within the characteristic time of oxidation by the hydroperoxide (see Supplementary Information Figure S1). This is consistent with the fact that reactions of Cys residues with this electrophile are much slower, and for instance, the oxidation rate constant of the single free Cys in human serum albumin has been reported as 30 $M^{-1}s^{-1}$.[53] The time course of enzyme´s intrinsic fluorescence change is shown in Figure 1 along with the dependence of the observed rate constant with the concentration of hydroperoxide (inset). The resulting rate constant was (6.0 ± 0.1) x $10^7$ $M^{-1}$ $s^{-1}$, 3-fold smaller than the one´s determined for 15-HpETE,[39] but 3~4 orders of magnitude larger compared to the reactivity of $H_2O_2$, *t*-BuOOH or CumeneOOH previously reported,[38, 39] These data confirm the significant preference of *Mt*AhpE for this type of substrates, suggesting that the length of the aliphatic tail may play a key-role in modulating the reactivity, being higher as longer is the carbon chain. Furthermore, hydroperoxide position in the aliphatic tail seems not to be so important for reactivity, since *Mt*AhpE oxidation by 12- and 15-HpETE occurred at similar rates (Table 1). A comparison of $Cys_P$ oxidation rate constant ($k_{ox}$) for a representative set of substrates is presented in Table 1.

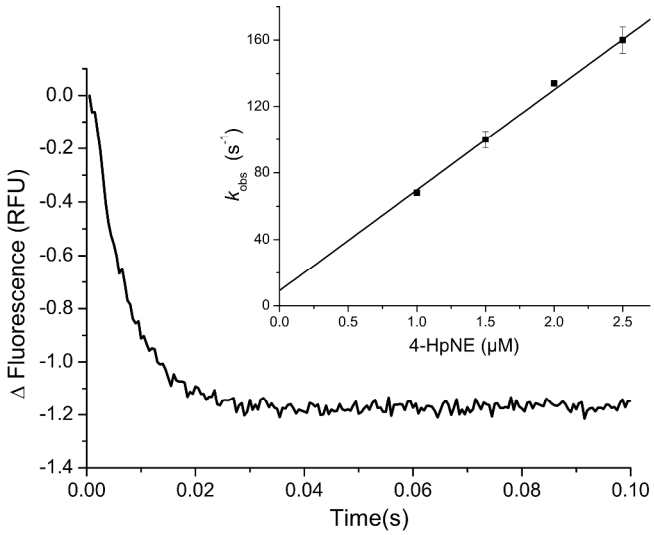


**Figure 1.** Kinetics of the oxidation of reduced *Mt*AhpE (0.1 μM) by 4-HpNE. Stopped-flow kinetics measurements were performed in 100 mM sodium phophate buffer plus 0.1 mM dtpa pH 7.4 and 25ºC and single exponential functions were fitted to the experimental data. Values of $k_{obs}$ obtained from these fittings are plotted as a function of 4-HpNE concentration (inset).

*Table 1. Mt*AhpE oxidation rate constants by various hydroperoxides.

| *Hydroperoxide* | *k ($M^{-1}s^{-1}$) pH 7.4, 25°C* | *Reference* |
|---|---|---|
| $H_2O_2$ | $8.2 \times 10^4$ | *38* |
| ONOOH | $1.9 \times 10^7$ | *38* |
| *t*-BuOOH | $8.0 \times 10^3$ | *39* |
| CumeneOOH | $4.0 \times 10^4$ | *39* |
| 4-HpNE | $6.0 \times 10^7$ | *This work* |
| 15-HpETE | $1.8 \times 10^8$ | *39* |
| 12-HpETE | $3.5 \times 10^8$ | *This work* |
| α-Linolenic acid hydroperoxides[a] | $2.7 \times 10^8$ | *39* |

[a]mixture of hydroperoxides formed from the lipoxygenase-catalyzed reaction

At this point, it is interesting to compare thermodynamics activation parameters of the reaction with fatty acid-derived hydroperoxides with those reported previously with $H_2O_2$.[19] To achieve this goal we have performed kinetics determinations at different temperatures. The results of the temperature dependence of the rate constant of *Mt*AhpE oxidation by 12-HpETE are shown in Figure 2. In Table 2 we report the thermodynamics activation parameters obtained by Eyring´s analysis of the data, compared with those ones determined previously for $H_2O_2$. Interestingly, the net decrease in $\Delta G^{\ddagger}$ for alkyl hydroperoxides is due to an entropic effect, which overcompensates the larger values observed for $\Delta H^{\ddagger}$ compared to $H_2O_2$. This is probably due to a subtle interplay among changes in protein-hydroperoxide interactions, protein dynamics (see below) and solvent effects.

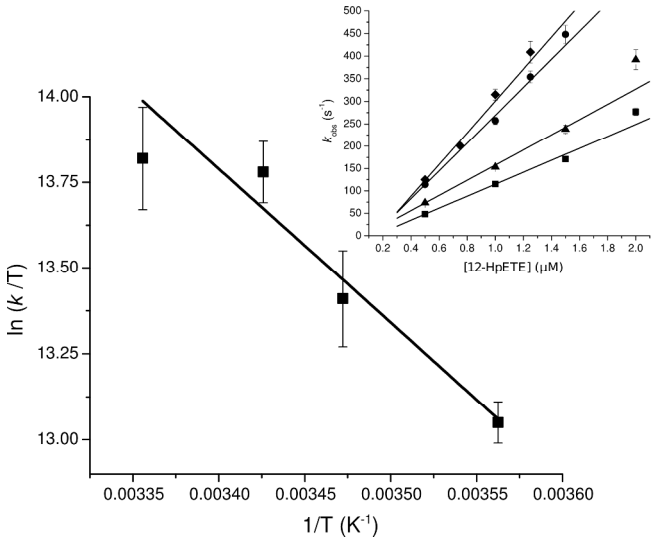


**Figure 2**. Determination of activation parameters of *Mt*AhpE oxidation by 12-HpETE. The activation parameters were calculated from Eyring plots of the rate constants obtained at different temperatures (mean values ± SD from 3 different experiments). Inset: $k_{obs}$ ($s^{-1}$) as a function of 12-HpETE concentration at T=7.7°C (■), 15°C (▲), 18.9°C (●) and 25°C (♦), as obtained in one independent experiment that was repeated three times with very similar results.

*Table 2.* Comparison of thermodynamics activation parameters of *Mt*AhpE oxidation by $H_2O_2$ and arachidonic acid derived hydroperoxide, obtained by temperature dependence Eyring´s analysis.

| *Hydroperoxide* | $\Delta H^{\ddagger}$(kcal/mol) | $\Delta S^{\ddagger}$ (cal/Kmol) | $\Delta G^{\ddagger}$(kcal/mol)[a] |
|---|---|---|---|
| $H_2O_2$[b] | 4.8 ± 0.5 | -19.1 ± 1.9 | 10.5 |
| 12-HpETE | 8.2 ± 0.3 | 8.0 ± 1.0 | 5.8 |

[a] calculated at 25°C
[b] taken from reference 19

*Hydrophobic patch characterization*

A structural and dynamical characterization of the reduced *Mt*AhpE shows an exposed hydrophobic region at the dimer interface, comprising non-polar sidechains from both subunits, which were pointed out as possible substrate interaction partners in the Michaelis complex, locating the peroxide in a reactive conformation.[39] In order to characterize this patch, we analyzed the interaction of the reduced enzyme with ANS.[54, 55] The use of this fluorescent probe has provided valuable information about the existence of hydrophobic pockets accessible from the solvent and with a nearby positive charge.[54] These binding sites promote the increase of ANS quantum yield with a concomitant blue shift of this emission. Among native proteins that exhibit this behavior, we can mention membrane proteins and a few water soluble fatty acid (or other hydrophobic ligands) binding proteins.[56, 57] We observed intrinsic fluorescence quenching with increasing amounts of ANS (Figure 3, inset) with the concomitant increase of ANS fluorescent quantum yield (see Supplementary Information Figure S2), both phenomena being dependent on ANS concentration. We used these properties to determine binding parameters for this interaction as described in Methods. Figure 3 shows the binding curves at three different

protein concentrations and the fitting of equation 1 to the experimental data. No significant differences were observed between the fittings to each series of data separately, and to the whole data set in a 3D global fitting (see Supplementary Information Table S1).

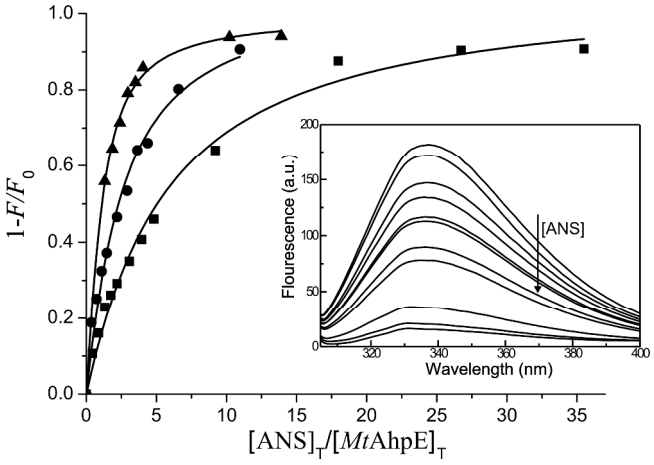


**Figure 3.** ANS binding isotherm using tryptophan FRET. Binding curves were determined at 25°C and pH 7.4. MtAhpE 1.5 μM (■), 3 μM (●) and 8 μM (▲), was incubated with increasing amounts of ANS. Total dilution was kept below 15%. Tryptophan quantum yield decrease was observed with $\lambda_{exc}$ = 295 nm and registering spectra between 305 and 400 nm as shown in the inset. Relative decrease of total fluorescence is plotted against $[ANS]_T/[MtAhpE]_T$. Equation 1 was fitted to the experimental data, with global fitting parameters values of n = 1.04 ± 0.01 and $K_a$ = (0.16 ± 0.02) $\mu M^{-1}$. The inset shows protein emission spectra for different ANS concentrations. The arrow indicates an increase of ANS concentration.

Analysis of binding curves shows a stoichiometry of one ANS equivalent per enzyme monomer with a thermodynamic association constant of (0.16 ± 0.02) $\mu M^{-1}$. These results confirm the presence of one exposed hydrophobic patch. Furthermore, the measured association constant is in the order of fatty acid binding proteins such as bovine serum albumin (0.32 $\mu M^{-1}$),[55] but does

not lay within the range of values usually attributed to the binding of ANS to molten globule-like states (1-5 x $10^{-2}$ $\mu M^{-1}$),[58] strongly suggesting the presence of a well-defined binding site.

*Substrate interaction with MtAhpE*

To obtain additional microscopic insights regarding the interaction of different substrates (*i.e.* $H_2O_2$, *t*-BuOOH, 4-HpNE and 15-HpETE) with the enzyme, we have employed a combination of docking and classical MD simulations. Specifically, we have performed 100 ns MD simulations, after a biased molecular docking to obtain the complexes starting structures as was described above. Peroxynitrous acid was not included in this comparative analysis as we have shown that the chemistry and reactivity of this peroxide could be somehow different compared to those tested herein.[59] As previously examined for $H_2O_2$,[19] in the *Michaelis* complex, the peroxide group interacts directly with different structural elements of the enzyme´s active site, producing a complex hydrogen bond network mainly involving reactive $Cys_{45}$, $Thr_{42}$ and $Arg_{116}$. These interactions locate the electrophilic $O_A$ in very close contact with the nucleophile ($S_P$), which was observed for the different substrates. Nonetheless, the non-reactive part of the longer chain substrates interacting with the enzyme, may also play an important role in the differential reactivity observed (consistent with the so called "Circe effect" initially described by Jencks when analyzing the catalytic mechanisms of enzymes).[60-62] Moreover, as the reactivity correlates with the length of the aliphatic chain of the hydroperoxides, we analyzed how this structural fact could modify substrate´s interaction. A comparison of the behavior of these hydroperoxides is presented in Figure 4.

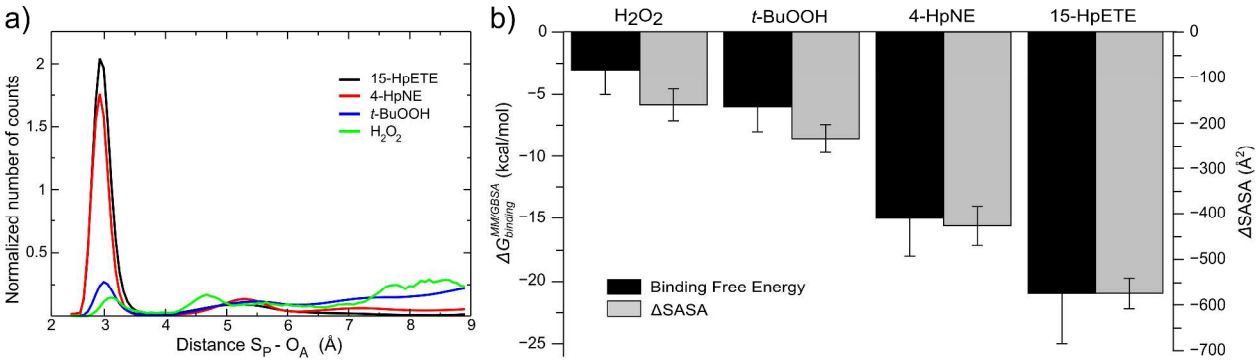


**Figure 4.** Interaction between *Mt*AhpE and different hydroperoxides. a) Reactive sulfur-oxygen distance distributions for different substrates. Normalized number of counts obtained from 100 ns long MDs, are plotted against $S_P$-$O_A$ distance. Results for 15-HpETE, 4-HpNE, *t*-BuOOH and $H_2O_2$ are depicted in black, red, blue and green lines respectively. b) MM/GBSA´s binding free energy in kcal mol$^{-1}$ (black bars, left axis) and calculated $\Delta$SASA in Å$^2$ (gray bars, right axis) are shown. Average values and standard deviation were calculated from a set of 200 structures.

The $S_P$-$O_A$ distance distribution is depicted in Figure 4a. Although all considered hydroperoxides show a probability maximum at about 3 Å, which is the reactive distance for this pair in the *Michaelis* complex, both 15-HpETE and 4-HpNE present very sharp distributions, with almost null frequency for any other distance longer than 3.5 Å, while smaller hydroperoxides such as $H_2O_2$ and *t*-BuOOH were likely to sample other non-reactive complexes conformations. This is mostly due to the collective interaction of the long aliphatic tail of 4-HpNE and 15-HpETE with the hydrophobic groove of *Mt*AhpE, which allows the peroxide group to tightly place into the active site. To further quantify this phenomena, we calculated binding free energies with the MM/GBSA scheme.[46] Even if the value itself may exhibit systematic errors, typically overestimated predictions, comparison of values for the same system with different substrates are meaningful.[63] Results show that binding free energies are 5 and 7 times larger for 4-HpNE and

15-HpETE than for $H_2O_2$, respectively (Figure 4b). Furthermore, as expected for this kind of collective hydrophobic interactions, the binding free energy correlates with surface area which is buried from water upon binding (*Δ*SASA, Figure 4b).

*Mt*AhpE´s $Cys_P$ is located at the N-terminus of helix α2, which place the sulfur atom approximately 10 Å away from the intersubunit interface of the dimer. As described by Li *et al.*,[40] this interface is characterized by a series of hydrophobic interactions between residues from both subunits. Furthermore, the interface region nearby $Cys_P$ presents several non-polar residues, giving place to the previously mentioned surface exposed hydrophobic patch. The structural and dynamical analysis of 4-HpNE and 15-HpETE interaction with the protein shows how the aliphatic carbon chains smoothly accommodate within the patch, maintaining numerous contacts with non-polar residues as $Ile_{13}$, $Pro_{38}$ and $Leu_{39}$ from $Cys_P$ subunit and $Pro_{74}$, $Pro_{75}$ and $Phe_{94}$ from the second subunit (Figure 5). The proximity between this hydrophobic region and $Cys_P$ allows this kind of substrates to lay most of their aliphatic carbon chains over the patch, supporting the direct interaction of the peroxide group with the reactive thiolate group.

In the structure of other members of the Prx family, such as PrxV and Tpx, a series of apolar residues surrounding the $Cys_P$ (the so called hydrophobic collar) have been identified and postulated to confer selectivity for organic hydroperoxides,[35] accounting for the ~$10^1$-$10^2$ times faster reaction of these enzymes with model organic peroxides like *t*-BuOOH or CumeneOOH than with $H_2O_2$.[33, 64] This is not the case for *Mt*AhpE, as the selectivity seems to be directed to long chain fatty acid derived peroxides and not model organic peroxides (see Table 1), due to the presence of the before mentioned hydrophobic patch, that involves apolar residues from the vicinity of $Cys_P$ up to ~15 Å away.

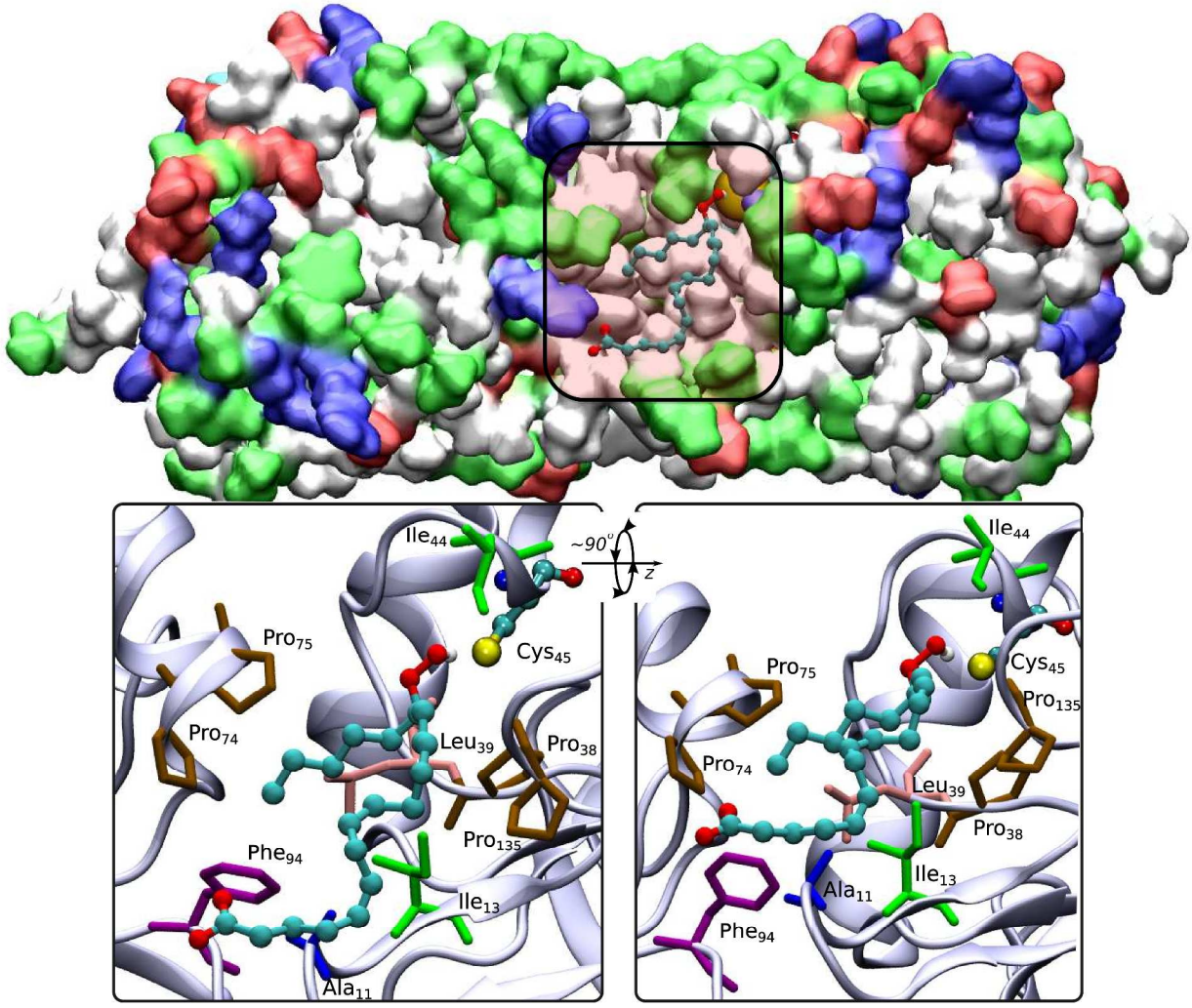


**Figure 5.** Typical snapshot of the MtAhpE:15-HpETE complex obtained by MD. Up: The molecular surface of reduced *Mt*AhpE is colored according to residue type (blue, basic; red, acidic; green, polar; white, nonpolar) and $Cys_P$ ($Cys_{45}$) is shown in yellow. Carbon atom of 15-HpETE are shown in cyan and oxygen ones in red. Down: Two detailed views of the interaction of the substrate within the hydrophobic groove. Important protein non-polar residues in the dimer interface are shown colored according to their identity. Only hydroperoxide's hydrogen atom is shown for clarity.

Besides locating the substrate in a reactive conformation, the interaction of fatty acid derived hydroperoxides with the previously described hydrophobic patch, affects the dynamical behavior of the enzyme. Figure 6 shows per residue root mean square fluctuations (rmsf) for the free protein, and the *Mt*AhpE:$H_2O_2$ and *Mt*AhpE:15-HpETE complexes. Residues mean fluctuations in the free system and in the complex with $H_2O_2$ are very similar, except for subtle changes including the reduction of mobility of some residues surrounding $Cys_P$ (residues 43-55 of subunit A). However, upon binding of 15-HpETE, significant changes are observed, not only involving the environment of $Cys_P$, which gets much more motionless, but also the decrease in flexibility of core parts of the enzyme like the central mixed β-sheet system, mostly β3 (Figure 6 top, blue areas), suggesting that this interaction significantly modifies dynamical aspects.

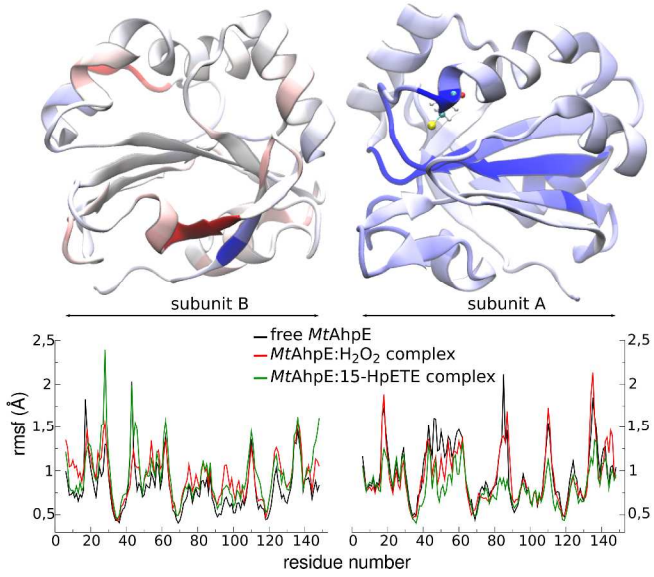


**Figure 6.** Protein fluctuation analysis. Down: root mean square fluctuations (rmsf) are plotted in a per residue basis for both dimer subunits for free *Mt*AhpE (black), *Mt*AhpE:$H_2O_2$ (red) and *Mt*AhpE:15-HpETE (green). Top: the structure of the dimer is colored from red (positive values) to blue (negative values) of the difference *Mt*AhpE:15-$HpETE_{rmsf}$ – free *Mt*$AhpE_{rmsf}$.

It is worth to notice that some changes are also appreciable in subunit B upon binding of 15-HpETE, which is not surprising as the hydrophobic patch involves residues from both subunits. The fluctuation behavior of subunit B is much more complex, as it did not show a general reduction of its mobility after binding such as subunit A, but some residues gain significant flexibility. This fact is related to the asymmetry between subunits frequently present in this kind of homo-oligomeric systems, as was previously discussed in Prxs.[65-68]

*Reaction mechanism*

Classical MD simulations afford valuable details regarding enzyme-substrate interaction, but cannot describe the reactive process. In order to do so, we have resorted to more sophisticated *state of the art* QM/MM simulations. Specifically, the molecular basis of the oxidation reaction of *Mt*AhpE by 15-HpETE were studied by QM/MM molecular dynamics simulations, using the *umbrella sampling* method in order to determine the free energy profile of the process as described above (Figure 7). This methodology was previously tested in similar systems, both in solution and catalyzed reactions.[18, 19] It is worth to notice that the estimation of the statistical error for activation and reaction free energies[51] of about ~1 kcal $mol^{-1}$, represents the error associated with the free energy profile determination. These errors may be underestimated due to incomplete sampling. However, our protocol includes a 2 ns long classical simulation before each QM/MM sampling window, which alleviates the sampling errors of typically too short QM/MM simulations. Representations of the reactant, transition and product states (*rs*, *ts* and *ps*) are depicted in Figure 8 (see Supplementary Information for details on the determined geometric parameters in Table S2 and a 3D animation of the trajectory of the reaction path).

The reaction is exergonic, with a reaction free energy change of (-35 ± 1) kcal $mol^{-1}$, in agreement with previously reported information for catalyzed and uncatalyzed reactions with other hydroperoxides.[18, 19] The activation free energy of (11 ± 1) kcal $mol^{-1}$, resulted 3 kcal $mol^{-1}$ lower than the obtained with the same methodology for $H_2O_2$,[19] consistent with the experimentally determined $\Delta\Delta G^{\ddagger}$ (see Table 2). This suggests that not only the formation of the complex may be important to explain this differential reactivity, but the reactive process after complex formation, may also present significant differences in terms of free energy barriers.

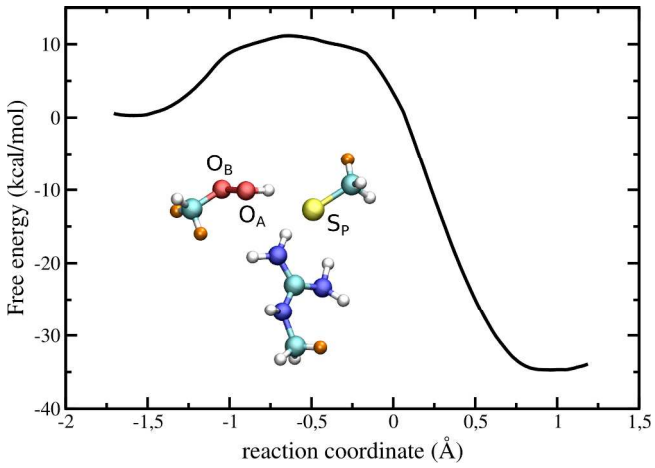


**Figure 7.** Free energy profile of the reduction of 15-HpETE by *Mt*AhpE obtained by QM/MM *umbrella sampling*. The QM subsystem is presented; link hydrogen atoms are shown in orange. The reaction coordinate was defined as the difference between the $O_A$-$O_B$ distance and the $S_P$-$O_A$ distance, and was sampled from -1.7 to 1.2 Å.

The *rs* is characterized by the peroxide group interacting with active site residues via hydrogen bonds, mainly $Thr_{42}$, $Cys_{45}$ and $Arg_{116}$, as has been determined for various members of the protein family by crystallographic studies.[20, 69] As reaction proceeds, the O-O peroxide bond enlarges with a concomitant continuous alignment of $O_B$, $O_A$ and $S_P$ atoms, until reaching the *ts*,

where the $O_B$-$O_A$-$S_P$ angle is practically 180°, the $O_B$-$O_A$ bond is 0.6 Å longer and $S_P$-$O_A$ distance is 0.4 Å shorter. At the *ts*, the complex hydrogen bond network is subtly redefined. The main difference is the establishment of a strong hydrogen bond interaction between $Thr_{42}$ and $O_A$ (see Figure 8 and Supplementary Information Table S2). As previously discussed, the numerous interactions that are present in this *ts*, are capable to stabilize this state in comparison with its homologue in aqueous solution.[20, 70]

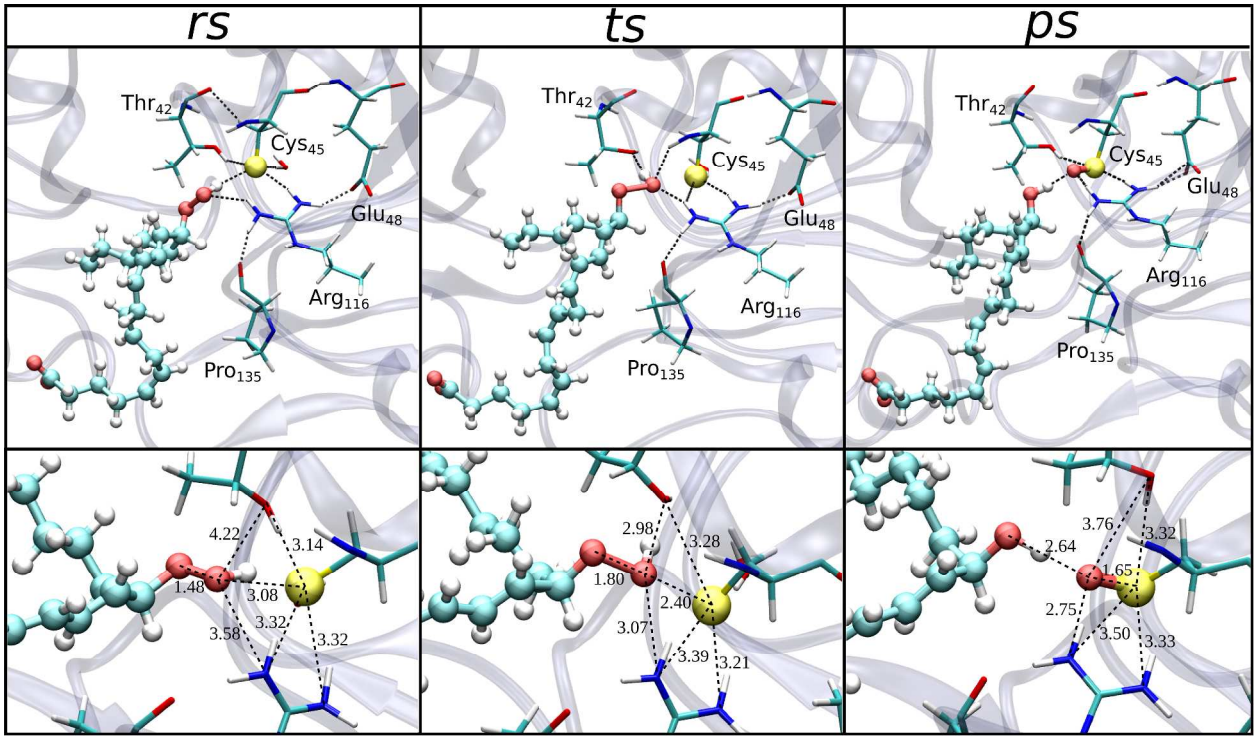


**Figure 8.** Upper panels: representative snapshots of reactants (rs), transition state (ts) and products (ps) for the reduction of 15-HpETE by *Mt*AhpE, obtained by *umbrella sampling* QM/MM simulations. Besides the reactive Cys ($Cys_{45}$) and the peroxide, the whole active site is shown, and relevant hydrogen bonds interactions are depicted. Lower panels: magnified views of the three states, where relevant distances are indicated.

Additionally, we also observe for this fatty acid-derived hydroperoxide, the same overall reaction mechanism reported for the reduction of $H_2O_2$ both in solution and by Prxs (the same sequence of covalent bond breaking and forming events),[18, 19] which involves a proton transfer from $O_A$ to $O_B$ that occurs after transition state. As a result, the *ps* shows the oxidized reactive $Cys_{45}$ in the unprotonated form of sulfenic acid ($Cys_{P\text{-}SO^-}$) and the protonated form of the corresponding arachidonic derived alcohol (Figure 8). The fact that the overall reduction mechanism for these kind of substrates is the same as the one described for $H_2O_2$,[19] agrees with the idea that the enzyme differential reactivity towards different peroxides is due to the influence of the "non-reactive" part of the substrate, that may affect the dynamical properties of the enzyme (Figure 6).

## CONCLUSIONS

We present an integrated experimental and theoretical study on the basis of comparative peroxide reduction by AhpE, the 1-Cys Prx from *Mycobacterium tuberculosis*. As described before,[38, 39] we confirmed that this enzyme present a clear preference for fatty acid- derived hydroperoxides, that could be endogenously generated by lipid peroxidation reactions through fatty acid-derived free radical production and propagation,[71, 72] or by lipoxygenase-catalyzed reactions.[73] A comparison of the activation parameters experimentally determined using different kind of substrates indicated that increased activation entropy is a major contributor to the faster reactivity of fatty acid hydroperoxides compared with $H_2O_2$. Furthermore, QM/MM calculations indicated that the overall mechanism of the reduction for the former substrates is the same as for $H_2O_2$, so the main reason of *Mt*AhpE specificity towards fatty acid hydroperoxides is that the substrate is anchored close to the enzyme´s active site via a hydrophobic interaction between the aliphatic sidechain and a hydrophobic patch at the entrance of the active site.

ANS flourimetric assays confirmed the presence of this surface exposed hydrophobic patch. The presence of this groove together with the properties of the aliphatic carbon chains of fatty acids, explains how these substrates can interact with the enzyme in a specific way, which accommodates the peroxide moiety into the active site, in a reactive position towards the thiolate group of $Cys_P$. Moreover, this interaction significantly modifies protein dynamics, restricting active site´s residues mobility, which might contribute to the increased catalytic efficiency.

Unfortunately, it has not been possible to measure peroxide binding for Prx systems (with the exception of a recent work on *Salmonella typhimurium* AhpC),[74] probably because the protein-substrate complex association is the rate limiting step during protein oxidation (*i.e.* the complex rapidly evolves to oxidized enzyme) under the considered experimental conditions.[13] However, computational simulations results suggest that both substrate binding and intrinsic reactivity are affected when going from $H_2O_2$ to fatty acid hydroperoxides. Specifically, computed binding free energies are indicative of tighter interactions, while the reaction free energy profiles are consistent with a greater reactivity of the latter substrates.

Prxs family exhibits a complex behavior in terms of substrate selectivity, with some members being more reactive towards $H_2O_2$, peroxynitrite or organic hydroperoxides.[75] Even though great progress has been made on the description of Prxs structure and function, the molecular basis underlying this variability, meaning how substrate´s and protein´s chemical properties could affect their reactivity, remains unclear. This study represents new insights on the understanding of the molecular factors that determines oxidizing substrate selectivity in this protein family.

ASSOCIATED CONTENT

**Supporting Information**. ANS additional results, kinetics controls, QM/MM´s geometric parameters and 3D animation specifications. This material is available free of charge via the Internet at http://pubs.acs.org.

AUTHOR INFORMATION

**Corresponding Authors**

* e-mail: dario@qi.fcen.uba.ar, Telephone: (5411)45763358, Fax: (5411)45763341; e-mail: madiat@fmed.edu.uy, Telephone: (5982)9249561, Fax: (5982)9249563.

**Present Addresses**

† German Institute of Human Nutrition, University of Potsdam, Germany.

**Author Contributions**

The manuscript was written through contributions of all authors. All authors have given approval to the final version of the manuscript.

‡ These authors contributed equally.

ACKNOWLEDGMENT

This work was partially supported by the Universidad de Buenos Aires (grant X074), CONICET, Centro de Biología Estructural Mercosur (CeBEM). MT and RR acknowledge the financial support of the Agencia Nacional de Investigación e Innovación (FCE_2011_1_5706, ANII, Uruguay) and Comisión Sectorial de Investigación Científica (CSIC), Universidad de la República and National Institutes of Health (R01 AI095173), respectively.

## ABBREVIATIONS

Prx, peroxiredoxin; Cys, L-cysteine; CysSOH, cysteine sulfenic acid; CysP, peroxidatic cysteine; ROS, reactive oxygen species; dtpa, diethylenetriaminepentaacetic acid; ANS, 1-anilino-8-naphthalene sulfonate; DTT, 1,4-dithiothreitol; arachidonic acid, 5Z,8Z,11Z,14Z-eicosatetraenoic acid; 12-HpETE, 12S-hydroperoxy-5Z,8Z,10E,14Z-eicosatetraenoic-5,6,8,9,11,12,14,15-d8 acid; 15-HpETE, 15S-hydroperoxy-5Z,8Z,11Z,13E-eicosatetraenoic acid; *t*-BuOOH, tert-butylhydroperoxide; CumeneOOH: cumene hydroperoxide; 4-HNE, 4-hydroxy-2E-nonenal;4-HpNE, 4-hydroperoxy-2E-nonenal ; DFT, density functional theory; QM, quantum mechanics; MM, molecular mechanics; MD, molecular dynamics; RMSF, root mean square fluctuation.

## REFERENCES


1. Han, Y. H., Kwon, J. H., Yu, D. Y., and Moon, E. Y. (2006) Inhibitory effect of peroxiredoxin II (Prx II) on Ras-ERK-NFkappaB pathway in mouse embryonic fibroblast (MEF) senescence, *Free Radical Research 40*, 1182-1189.
2. Kim, H., Lee, T. H., Park, E. S., Suh, J. M., Park, S. J., Chung, H. K., Kwon, O. Y., Kim, Y. K., Ro, H. K., and Shong, M. (2000) Role of peroxiredoxins in regulating intracellular hydrogen peroxide and hydrogen peroxide-induced apoptosis in thyroid cells, *Journal of Biological Chemistry 275*, 18266-18270.
3. Park, J., Lee, S., and Kang, S. W. (2014) 2-cys peroxiredoxins: emerging hubs determining redox dependency of Mammalian signaling networks, *International Journal of Cell Biology 2014*, 715867-715876.
4. Randall, L. M., Ferrer-Sueta, G., and Denicola, A. (2013) Peroxiredoxins as preferential targets in H2O2-induced signaling, *Methods in enzymology 527*, 41-63.
5. Rhee, S. G., Chae, H. Z., and Kim, K. (2005) Peroxiredoxins: a historical overview and speculative preview of novel mechanisms and emerging concepts in cell signaling, *Free Radical Biology and Medicine 38*, 1543-1552.
6. Ummanni, R., Barreto, F., Venz, S., Scharf, C., Barett, C., Mannsperger, H. A., Brase, J. C., Kuner, R., Schlomm, T., Sauter, G., Sultmann, H., Korf, U., Bokemeyer, C., Walther, R., Brummendorf, T. H., and Balabanov, S. (2012) Peroxiredoxins 3 and 4 are overexpressed in prostate cancer tissue and affect the proliferation of prostate cancer cells in vitro, *Journal of Proteome Research 11*, 2452-2466.
7. Dons, L. E., Mosa, A., Rottenberg, M. E., Rosenkrantz, J. T., Kristensson, K., and Olsen, J. E. (2014) Role of the Listeria monocytogenes 2-Cys peroxiredoxin homologue in protection against oxidative and nitrosative stress and in virulence, *Pathogens and Disease 70*, 70-74.

8. Kaihami, G. H., Almeida, J. R., Santos, S. S., Netto, L. E., Almeida, S. R., and Baldini, R. L. (2014) Involvement of a 1-Cys peroxiredoxin in bacterial virulence, *PLoS Pathogens 10*, e1004442.
9. Li, L., and Yu, A. Q. (2015) The functional role of peroxiredoxin 3 in reactive oxygen species, apoptosis, and chemoresistance of cancer cells, *Journal of Cancer Research and Clinical Oncology*, 1-7.
10. Piacenza, L., Zago, M. P., Peluffo, G., Alvarez, M. N., Basombrio, M. A., and Radi, R. (2009) Enzymes of the antioxidant network as novel determiners of Trypanosoma cruzi virulence, *International Journal for Parasitology 39*, 1455-1464.
11. Song, I. S., Kim, H. K., Jeong, S. H., Lee, S. R., Kim, N., Rhee, B. D., Ko, K. S., and Han, J. (2011) Mitochondrial peroxiredoxin III is a potential target for cancer therapy, *International Journal of Molecular Sciences 12*, 7163-7185.
12. Poole, L. B. (2007) The catalytic mechanism of peroxiredoxins, *Subcellular Biochemistry 44*, 61-81.
13. Trujillo, M., Ferrer-Sueta, G., Thomson, L., Flohe, L., and Radi, R. (2007) Kinetics of peroxiredoxins and their role in the decomposition of peroxynitrite, *Subcellular Biochemistry 44*, 83-113.
14. Trujillo, M., Ferrer-Sueta, G., and Radi, R. (2008) Kinetic studies on peroxynitrite reduction by peroxiredoxins, *Methods in Enzymology 441*, 173-196.
15. Hofmann, B., Hecht, H. J., and Flohe, L. (2002) Peroxiredoxins, *Biological Chemistry 383*, 347-364.
16. Sobotta, M. C., Liou, W., Stöcker, S., Talwar, D., Oehler, M., Ruppert, T., Scharf, A. N. D., and Dick, T. P. (2015) Peroxiredoxin-2 and STAT3 form a redox relay for H2O2 signaling, *Nature Chemical Biology 11*, 64-70.
17. Edwards, J. O. (1962) Nucleophillic displacement on oxygen in peroxides, In *Peroxide reaction mechanisms* (Edwards, J. O., Ed.), pp 67-106, Interscience, New York.
18. Zeida, A., Babbush, R., González Lebrero, M. C., Trujillo, M., Radi, R., and Estrin, D. A. (2012) Molecular basis of the mechanism of thiol oxidation by hydrogen peroxide in aqueous solution: challenging the SN2 paradigm, *Chemical Research in Toxicology 25*, 741-746.
19. Zeida, A., Reyes, A. M., González Lebrero, M. C., Radi, R., Trujillo, M., and Estrin, D. A. (2014) The extraordinary catalytic ability of peroxiredoxins: a combined experimental and QM/MM study on the fast thiol oxidation step, *Chemical Communications 50*, 10070-10073.
20. Hall, A., Parsonage, D., Poole, L. B., and Karplus, P. A. (2010) Structural evidence that peroxiredoxin catalytic power is based on transition-state stabilization, *Journal of Molecular Biology 402*, 194-209.
21. Nagy, P., Karton, A., Betz, A., Peskin, A. V., Pace, P., O'Reilly, R. J., Hampton, M. B., Radom, L., and Winterbourn, C. C. (2011) Model for the exceptional reactivity of peroxiredoxins 2 and 3 with hydrogen peroxide: A kinetic and computational study, *Journal of Biological Chemistry 286*, 18048-18055.
22. Portillo-Ledesma, S., Sardi, F., Manta, B., Tourn, M. V., Clippe, A., Knoops, B., Alvarez, B., Coitino, E. L., and Ferrer-Sueta, G. (2014) Deconstructing the catalytic efficiency of peroxiredoxin-5 peroxidatic cysteine, *Biochemistry 53*, 6113-6125.
23. Nelson, K. J., Knutson, S. T., Soito, L., Klomsiri, C., Poole, L. B., and Fetrow, J. S. (2011) Analysis of the peroxiredoxin family: using active-site structure and sequence information for global classification and residue analysis, *Proteins: Structure, Function, and Bioinformatics 79*, 947-964.
24. Soito, L., Williamson, C., Knutson, S. T., Fetrow, J. S., Poole, L. B., and Nelson, K. J. (2011) PREX: PeroxiRedoxin classification indEX, a database of subfamily assignments across the diverse peroxiredoxin family, *Nucleic Acids Research 39*, D332-D337.

25. Aden, J., Wallgren, M., Storm, P., Weise, C. F., Christiansen, A., Schroder, W. P., Funk, C., and Wolf-Watz, M. (2011) Extraordinary μs-ms backbone dynamics in Arabidopsis thaliana peroxiredoxin Q, *Biochimica et Biophysica Acta (BBA) - General Subjects 1814*, 1880-1890.
26. Trindade, D. F., Cerchiaro, G., and Augusto, O. (2006) A role for peroxymonocarbonate in the stimulation of biothiol peroxidation by the bicarbonate/carbon dioxide pair, *Chemical Research in Toxicology 19*, 1475-1482.
27. Bryk, R., Griffin, P., and Nathan, C. (2000) Peroxynitrite reductase activity of bacterial peroxiredoxins, *Nature 407*, 211-215.
28. Manta, B., Hugo, M., Ortiz, C., Ferrer-Sueta, G., Trujillo, M., and Denicola, A. (2009) The peroxidase and peroxynitrite reductase activity of human erythrocyte peroxiredoxin 2, *Archives of Biochemistry and Biophysics 484*, 146-154.
29. Ogusucu, R., Rettori, D., Munhoz, D. C., Netto, L. E., and Augusto, O. (2007) Reactions of yeast thioredoxin peroxidases I and II with hydrogen peroxide and peroxynitrite: rate constants by competitive kinetics, *Free Radical Biology and Medicine 42*, 326-334.
30. Parsonage, D., Karplus, P. A., and Poole, L. B. (2008) Substrate specificity and redox potential of AhpC, a bacterial peroxiredoxin, *Proceedings of the National Academy of Sciences 105*, 8209-8214.
31. Pineyro, M. D., Arcari, T., Robello, C., Radi, R., and Trujillo, M. (2011) Tryparedoxin peroxidases from Trypanosoma cruzi: high efficiency in the catalytic elimination of hydrogen peroxide and peroxynitrite, *Archives of Biochemistry and Biophysics 507*, 287-295.
32. Dubuisson, M., Vander Stricht, D., Clippe, A., Etienne, F., Nauser, T., Kissner, R., Koppenol, W. H., Rees, J. F., and Knoops, B. (2004) Human peroxiredoxin 5 is a peroxynitrite reductase, *FEBS Letters 571*, 161-165.
33. Trujillo, M., Clippe, A., Manta, B., Ferrer-Sueta, G., Smeets, A., Declercq, J. P., Knoops, B., and Radi, R. (2007) Pre-steady state kinetic characterization of human peroxiredoxin 5: Taking advantage of Trp84 fluorescence increase upon oxidation, *Archives of Biochemistry and Biophysics 467*, 95-106.
34. Baker, L. M., and Poole, L. B. (2003) Catalytic mechanism of thiol peroxidase from Escherichia coli. Sulfenic acid formation and overoxidation of essential CYS61, *Journal of Biological Chemistry 278*, 9203-9211.
35. Perkins, A., Poole, L. B., and Karplus, P. A. (2014) Tuning of peroxiredoxin catalysis for various physiological roles, *Biochemistry 53*, 7693-7705.
36. Declercq, J. P., Evrard, C., Clippe, A., Stricht, D. V., Bernard, A., and Knoops, B. (2001) Crystal structure of human peroxiredoxin 5, a novel type of mammalian peroxiredoxin at 1.5 A resolution, *Journal of Molecular Biology 311*, 751-759.
37. Flohé, L., Toppo, S., Cozza, G., and Ursini, F. (2010) A Comparison of Thiol Peroxidase Mechanisms, *Antioxidants & Redox Signaling 15*, 763-780.
38. Hugo, M., Turell, L., Manta, B., Botti, H., Monteiro, G., Netto, L. E., Alvarez, B., Radi, R., and Trujillo, M. (2009) Thiol and sulfenic acid oxidation of AhpE, the one-cysteine peroxiredoxin from Mycobacterium tuberculosis: kinetics, acidity constants, and conformational dynamics, *Biochemistry 48*, 9416-9426.
39. Reyes, A. M., Hugo, M., Trostchansky, A., Capece, L., Radi, R., and Trujillo, M. (2011) Oxidizing substrate specificity of Mycobacterium tuberculosis alkyl hydroperoxide reductase E: Kinetics and mechanisms of oxidation and overoxidation, *Free Radical Biology and Medicine 51*, 464-473.
40. Li, S., Peterson, N. A., Kim, M. Y., Kim, C. Y., Hung, L. W., Yu, M., Lekin, T., Segelke, B. W., Lott, J. S., and Baker, E. N. (2005) Crystal structure of AhpE from Mycobacterium tuberculosis, a 1-Cys peroxiredoxin, *Journal of Molecular Biology 346*, 1035-1046.
41. Gasteiger, E., Hoogland, C., Gattiker, A., Wilkins, M. R., Appel, R. D., and Bairoch, A. (2005) *Protein identification and analysis tools on the ExPASy server*, Springer.

42. DeGray, J. A., Gunther, M. R., Tschirret-Guth, R., Ortiz de Montellano, P. R., and Mason, R. P. (1997) Peroxidation of a specific tryptophan of metmyoglobin by hydrogen peroxide, *The Journal of Biological Chemistry 272*, 2359-2362.
43. Jorgensen, W. L., Chandrasekhar, J., Madura, J. D., Impey, R. W., and Klein, M. L. (1983) Comparison of simple potential functions for simulating liquid water, *The Journal of Chemical Physics 79*, 926-935.
44. Pearlman, D. A., Case, D. A., Caldwell, J. W., Ross, W. S., Cheatham, T. E., DeBolt, S., Ferguson, D., Seibel, G., and Kollman, P. (1995) AMBER, a package of computer programs for applying molecular mechanics, normal mode analysis, molecular dynamics and free energy calculations to simulate the structural and energetic properties of molecules, *Computer Physics Communications 91*, 1-41.
45. Gauto, D. F., Di Lella, S., Guardia, C. M. A., Estrin, D. A., and Martí, M. A. (2009) Carbohydrate-binding proteins: Dissecting ligand structures through solvent environment occupancy, *Journal of Physical Chemistry B 113*, 8717-8724.
46. Rastelli, G., Rio, A. D., Degliesposti, G., and Sgobba, M. (2010) Fast and accurate predictions of binding free energies using MM-PBSA and MM-GBSA, *Journal of Computational Chemistry 31*, 797-810.
47. González Lebrero, M. C., and Estrin, D. A. (2007) QM-MM investigation of the reaction of peroxynitrite with carbon dioxide in water, *Journal of Chemical Theory and Computation 3*, 1405-1411.
48. Nitsche, M. A., Ferreria, M., Mocskos, E. E., and González Lebrero, M. C. (2014) GPU accelerated implementation of density functional theory for hybrid QM/MM simulations, *Journal of Chemical Theory and Computation 10*, 959-967.
49. Crespo, A., Scherlis, D. A., Martí, M. A., Ordejón, P., Roitberg, A. E., and Estrin, D. A. (2003) A DFT-Based QM-MM Approach Designed for the Treatment of Large Molecular Systems: Application to Chorismate Mutase, *The Journal of Physical Chemistry B 107*, 13728-13736.
50. Kästner, J., and Thiel, W. (2005) Bridging the gap between thermodynamic integration and umbrella sampling provides a novel analysis method:"Umbrella integration", *The Journal of Chemical Physics 123*, 144104.
51. Kästner, J., and Thiel, W. (2006) Analysis of the statistical error in umbrella sampling simulations by umbrella integration, *The Journal of Chemical Physics 124*, 234106.
52. Humphrey, W., Dalke, A., and Schulten, K. (1996) VMD: Visual molecular dynamics, *Journal of Molecular Graphics 14*, 33-38.
53. Aldini, G., Regazzoni, L., Orioli, M., Rimoldi, I., Facino, R. M., and Carini, M. (2008) A tandem MS precursor-ion scan approach to identify variable covalent modification of albumin Cys34: a new tool for studying vascular carbonylation, *Journal of Mass Spectrometry 43*, 1470-1481.
54. Matulis, D., and Lovrien, R. (1998) 1-anilino-8-naphthalene sulfonate anion-protein binding depends primarily on ion pair formation, *Biophysical Journal 74*, 422-429.
55. Cattoni, D. I., Kaufman, S. B., and González Flecha, F. L. (2009) Kinetics and thermodynamics of the interaction of 1-anilino-naphthalene-8-sulfonate with proteins, *Biochimica et Biophysica Acta (BBA) - Proteins and Proteomics 1794*, 1700-1708.
56. Collini, M., D'Alfonso, L., Molinari, H., Ragona, L., Catalano, M., and Baldini, G. (2003) Competitive binding of fatty acids and the fluorescent probe 1-8-anilinonaphthalene sulfonate to bovine β-lactoglobulin, *Protein Science 12*, 1596-1603.
57. Roman, E. A., Argüello, J. M., and González Flecha, F. L. (2010) Reversible unfolding of a thermophilic membrane protein in phospholipid/detergent mixed micelles, *Journal of Molecular Biology 397*, 550-559.
58. Shi, L., Palleros, D. R., and Fink, A. L. (1994) Protein conformational changes induced by 1,1'-Bis(4-anilino-5-naphthalenesulfonic acid): Preferential binding to the molten globule of DnaK, *Biochemistry 33*, 7536-7546.

59. Zeida, A., González Lebrero, M. C., Radi, R., Trujillo, M., and Estrin, D. A. (2013) Mechanism of cysteine oxidation by peroxynitrite: An integrated experimental and theoretical study, *Archives of Biochemistry and Biophysics 539*, 81-86.
60. Moore, S., and Jencks, W. (1982) Formation of active site thiol esters of CoA transferase and the dependence of catalysis on specific binding interactions, *The Journal of Biological Chemistry 257*, 10893.
61. Jencks, W. P. (1994) Reaction mechanisms, catalysis, and movement, *Protein Science 3*, 2459-2464.
62. Wu, N., Mo, Y., Gao, J., and Pai, E. F. (2000) Electrostatic stress in catalysis: Structure and mechanism of the enzyme orotidine monophosphate decarboxylase, *Proceedings of the National Academy of Sciences 97*, 2017-2022.
63. Hou, T., Wang, J., Li, Y., and Wang, W. (2010) Assessing the performance of the MM/PBSA and MM/GBSA methods. 1. The accuracy of binding free energy calculations based on molecular dynamics simulations, *Journal of Chemical Information and Modeling 51*, 69-82.
64. Hall, A., Sankaran, B., Poole, L. B., and Karplus, P. A. (2009) Structural changes common to catalysis in the Tpx peroxiredoxin subfamily, *Journal of Molecular Biology 393*, 867-881.
65. Salsbury, F. R., Yuan, Y., Knaggs, M. H., Poole, L. B., and Fetrow, J. S. (2012) Structural and electrostatic asymmetry at the active site in typical and atypical peroxiredoxin dimers, *The Journal of Physical Chemistry B 116*, 6832-6843.
66. Yuan, Y., Knaggs, M. H., Poole, L. B., Fetrow, J. S., and Salsbury, F. R. (2010) Conformational and oligomeric effects on the cysteine pKa of tryparedoxin peroxidase, *Journal of Biomolecular Structure and Dynamics 28*, 51-70.
67. Budde, H., Flohé, L., Hecht, H.-J., Hofmann, B., Stehr, M., Wissing, J., and Lünsdorf, H. (2003) Kinetics and redox-sensitive oligomerisation reveal negative subunit cooperativity in tryparedoxin peroxidase of Trypanosoma brucei brucei, *Biological Chemistry 384*, 619-633.
68. Haynes, A. C., Qian, J., Reisz, J. A., Furdui, C. M., and Lowther, W. T. (2013) Molecular basis for the resistance of human mitochondrial 2-Cys peroxiredoxin 3 to hyperoxidation, *Journal of Biological Chemistry 288*, 29714-29723.
69. Nakamura, T., Kado, Y., Yamaguchi, T., Matsumura, H., Ishikawa, K., and Inoue, T. (2010) Crystal structure of peroxiredoxin from Aeropyrum pernix K1 complexed with its substrate, hydrogen peroxide, *Journal of Biochemistry 147*, 109-115.
70. Hall, A., Nelson, K., Poole, L. B., and Karplus, P. A. (2011) Structure-based insights into the catalytic power and conformational dexterity of peroxiredoxins, *Antioxidants & Redox Signaling 15*, 795-815.
71. Porter, N., Caldwell, S., and Mills, K. (1995) Mechanisms of free radical oxidation of unsaturated lipids, *Lipids 30*, 277-290.
72. Radi, R., Beckman, J. S., Bush, K. M., and Freeman, B. A. (1991) Peroxynitrite-induced membrane lipid peroxidation: The cytotoxic potential of superoxide and nitric oxide, *Archives of Biochemistry and Biophysics 288*, 481-487.
73. Bonney, R. J., Opas, E. E., and Humes, J. L. (1985) Lipoxygenase pathways of macrophages, *Federation Proceedings 44*, 2933-2936.
74. Parsonage, D., Nelson, K. J., Ferrer-Sueta, G., Alley, S., Karplus, P. A., Furdui, C. M., and Poole, L. B. (2015) Dissecting peroxiredoxin catalysis: Separating binding, peroxidation, and resolution for a bacterial AhpC, *Biochemistry 54*, 1567-1575.
75. Ferrer-Sueta, G., Manta, B., Botti, H., Radi, R., Trujillo, M., and Denicola, A. (2011) Factors affecting protein thiol reactivity and specificity in peroxide reduction, *Chemical Research in Toxicology 24*, 434-450.

For Table of Contents Use Only:

Molecular basis of hydroperoxide specificity in peroxiredoxins: the case of AhpE from

*Mycobacterium tuberculosis*

*Ari Zeida, Aníbal M. Reyes, Pablo Lichtig, Martín Hugo, Diego S. Vazquez, Javier Santos, F. Luis González Flecha, Rafael Radi, Dario A. Estrin, Madia Trujillo*